ungeranlygeranylated forms but the effects on Ras depended on cell types. Interestingly, ZOL-treated cells showed increase in total amounts of RhoA, Rac1 and less significantly Cdc42 but not Rab6, which were probably caused by a feedback mechanism in Rho family proteins production because of the decreased functional membrane-bound proteins (Supplementary Figure S2).

Involvement of geranylgeranylated small G proteins in apoptosis or S-phase arrest. We used inhibitors or siRNA for respective small G proteins to identify possible small G proteins that were involved in ZOL-induced apoptosis or S-phase arrest (Figure 2). C3 transferase, an inhibitor of RhoA, did not influence an expression level of total RhoA in contrast to ZOL treatments, but decreased that of the GTP-binding form (Figure 2a). Cell cycle analyses showed that C3 transferase increased sub-G1 populations in MSTO-211H cells, and augmented G2/M-phase but not S-phase fractions in EHMES-10 cells (Figure 2b). NSC23766, an inhibitor of Rac1, which decreased the level of GTP-binding Rac1 without upregulating the whole protein level, did not influence on cell cycle in both MSTO-211H and EHMES-10 cells (Figures 2c and d). In contrast, ZOL treatments increased the whole and GTP-binding Rac1 as in the case of elevated whole RhoA expression. We used siRNA to downregulate Cdc42 protein expression because Cdc42 inhibitor was unavailable (Figure 2e). The siRNA for Cdc42 suppressed the protein expression, but did not influence cell cycle of MSTO-211H and EHMES-10 cells (Figure 2f). These data indicated that inhibition of RhoA but not Rac1 or Cdc42 functions induced apoptosis in MSTO-211H cells and none of the inhibition was associated with S-phase arrest in EHMES-10 cells.

We further investigated the effects of inhibitors for geranylgeranylation, GGTI-298 and NE10790, which inhibit geranylgeranyl transferase I and II, respectively (Supplementary Figure S1). GGTI-298 treatments increased unprenylated Rap1A and whole RhoA levels as shown in ZOL-treated cells, but did not influence Rab6 expression (Figure 3a). The majority of RhoA in GGTI-298-treated cells was distributed in cytoplasmic fractions but that of Rab6 remained in membrane fractions (Figures 3b and c). In addition, GGTI-298 treatments upregulated Rac1 expression with enhanced GTP-binding Rac1 in MSTO-211H and less significantly in EHMES-10 cells (Figure 2c). NE10790 treatments did not influence the levels of unprenylated Rap1A or total RhoA expression, or fractionated RhoA distributions (Figures 3a–c). In contrast, NE10790-treated cells showed downregulation of Rab6 translocation to membrane in MSTO-211H and EHMES-10 cells although the expression levels were variable depending on the cells tested. We also examined cell cycle progression with these inhibitors. GGTI-298 increased sub-G1 populations in time- and

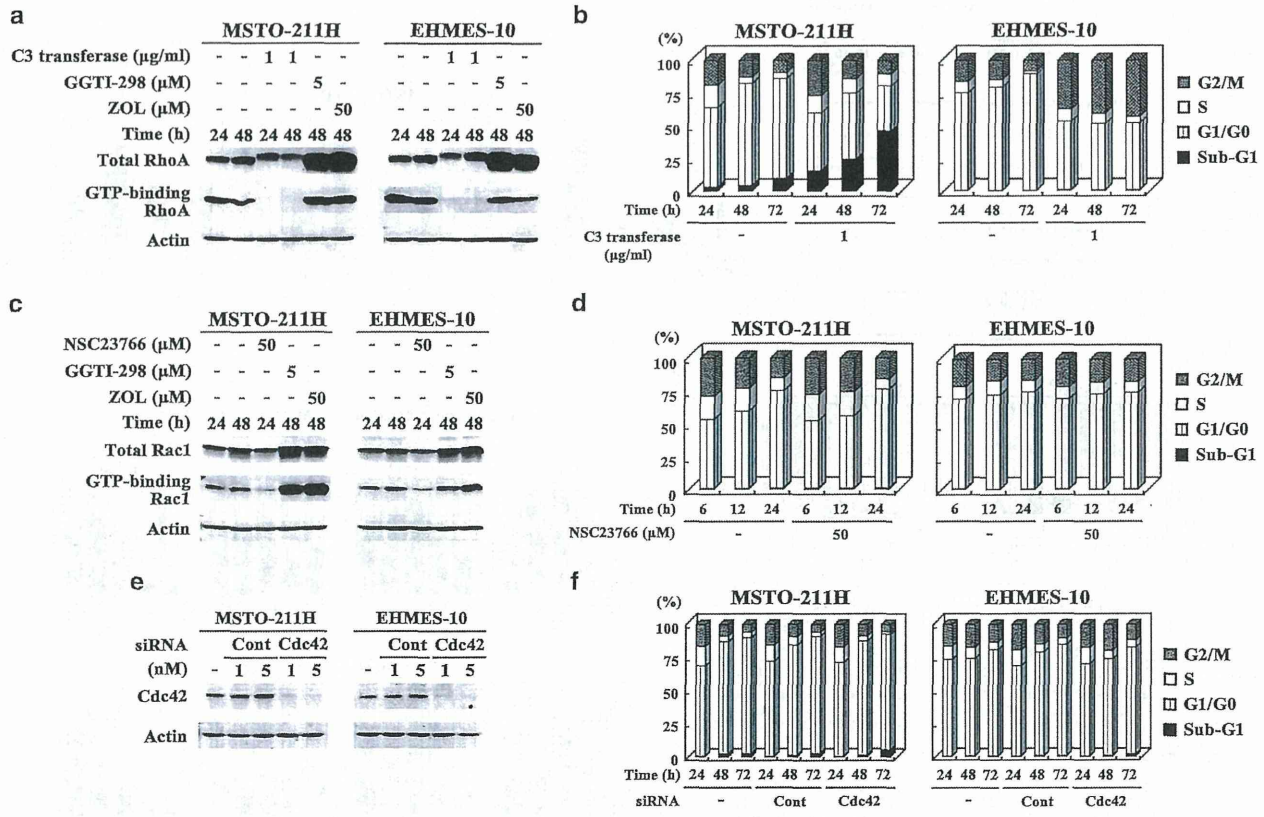

Figure 2 Influence of Rho inhibition on cell cycle. (**a**, **c** and **e**) Cells treated with an inhibitor as indicated, or transfected with Cdc42-siRNA or control-siRNA (Cont) were subjected to western blot analyses. (**b**, **d** and **f**) Cells were treated with C3 transferase (**b**) or NSC23766 (**d**), or transfected with 5 nM siRNA (**f**), and then were examined for cell cycle with flow cytometry

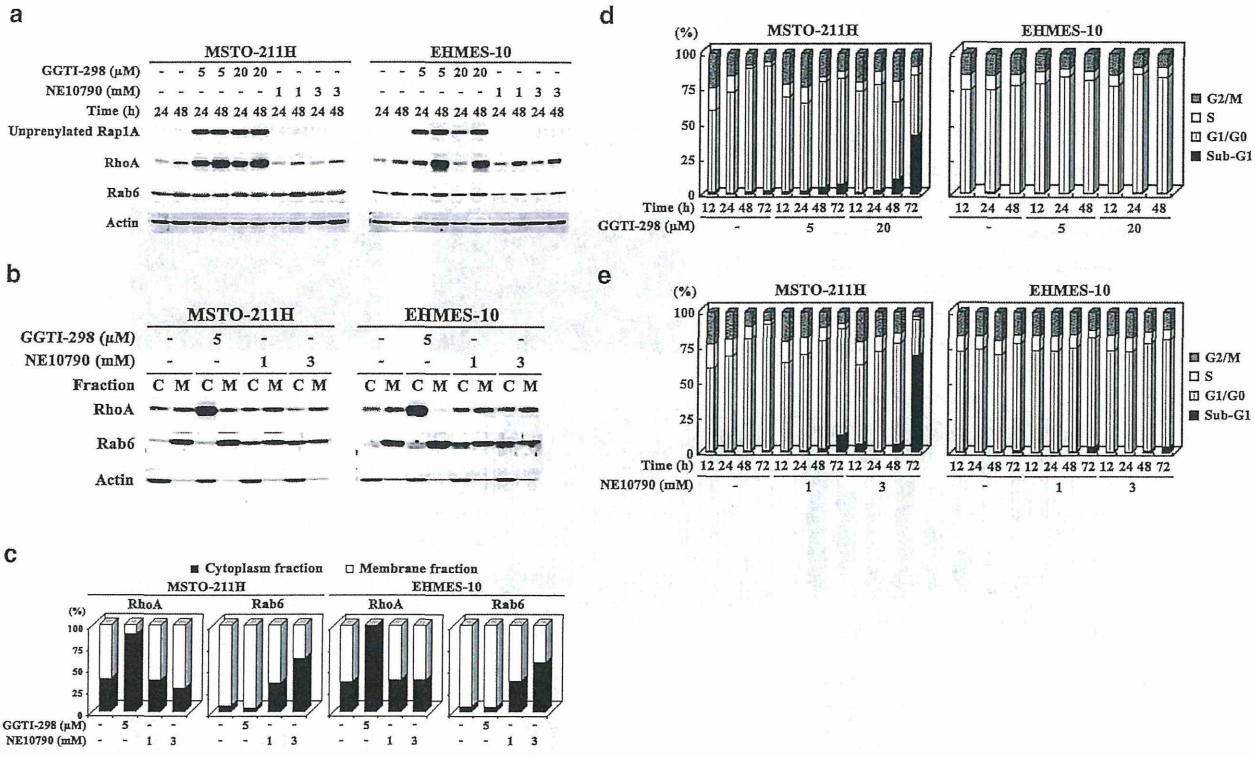

Figure 3 Influence of geranylgeranyl transferase I and II inhibition on cell cycle. (**a**) Cells treated with agents as indicated were subjected to western blot analyses. (**b**) Lysates of cells treated with agents for 48 h were separated into cytoplasm (c) or membrane (m) fraction and probed with respective antibodies. (**c**) Differential expression ratios between cytoplasm and membrane fractions in (**b**) were determined with an imaging analyzer. (**d** and **e**) Cells treated with agents as indicated were examined for cell cycle with flow cytometry

dose-dependent manners in MSTO-211H cells but scarcely influenced the cell cycle in EHMES-10 cells (Figure 3d). NE10790 also augmented sub-G1 fractions in MSTO-211H cells but had little effects on cell cycle in EHMES-10 cells (Figure 3e). These data indicated that ungeranylgeranylation of Rho and/or Rab family proteins was responsible for ZOL-induced apoptosis but not for S-phase arrest.

Apoptosis mediated by inhibited Rab functions and S-phase arrest by suppressed Topo II activity. We investigated a possible mechanism of apoptosis induction by the inhibitors that increased sub-G1 fractions in MSTO-211H cells, C3 transferase, GGTI-298 and NE10790 (Figure 4a). C3 transferase-treated cells showed minimal cleavage of PARP without caspase-3 and -9 cleavages, and did not change Mcl-1 or phosphorylated Akt levels. GGTI-298-treated cells transiently downregulated the phosphorylation of Akt levels and minimally Mcl-1 levels, but did not induce cleavages of caspase-9, -3 or PARP. In contrast, NE10790 treatments decreased both phosphorylated Akt and Mcl-1 levels, and induced cleavages of caspase-9, -3 and PARP, all of which changes were the same as those observed in ZOL-treated MSTO-211H cells. These data collectively suggested that ZOL-induced apoptosis was attributable to the inhibition of Rab family proteins.

We investigated a possible mechanism of ZOL-induced S-phase arrest in EHMES-10 cells. We firstly examined topoisomerase (Topo) II activities in ZOL-treated cells (Figure 4b). Cell extracts of untreated MSTO-211H and EHMES-10 cells altered catenated kinetoplast DNA into decatenated form, demonstrating that the cells contained an endogenous Topo II activity. In contrast, extracts from ZOL-treated cells maintained catenated kinetoplast DNA form as shown in those from cells treated with etoposide (ETO), a Topo II inhibitor. We next analyzed cell cycle of ETO-treated MSTO-211H and EHMES-10 cells (Figure 4c). ETO treatments augmented sub-G1 fractions in MSTO-211H cells and upregulated S- and G2/M-phase populations in EHMES-10 cells. We further investigated whether ZOL inhibited Topo I activities with an assay to detect relaxation of supercoiled DNA (Figure 4d). Extracts of untreated MSTO-211H and EHMES-10 cells induced the relaxation of supercoiled DNA, demonstrating that they had an endogenous Topo I activity. ETO treatments also induced the relaxation because ETO was a specific Topo II inhibitor, and ZOL-treated cells had a minimal inhibitory activity to relax supercoiled DNA only at 72 h incubation. In contrast, cells treated with topotecan, a Topo I inhibitor, showed an inhibitory action on relaxing supercoiled DNA (Figure 4e). These data demonstrated that ZOL inhibited Topo II but scarcely Topo I activity and suggested that the blocking of Topo II activity was responsible for apoptosis in MSTO-211H cells and for S-phase arrest in EHMES-10 cells.

ZOL-mediated morphological changes by inhibition of RhoA and Cdc42. Cells treated with ZOL showed morphological changes, altering fibroblastic into round-shaped

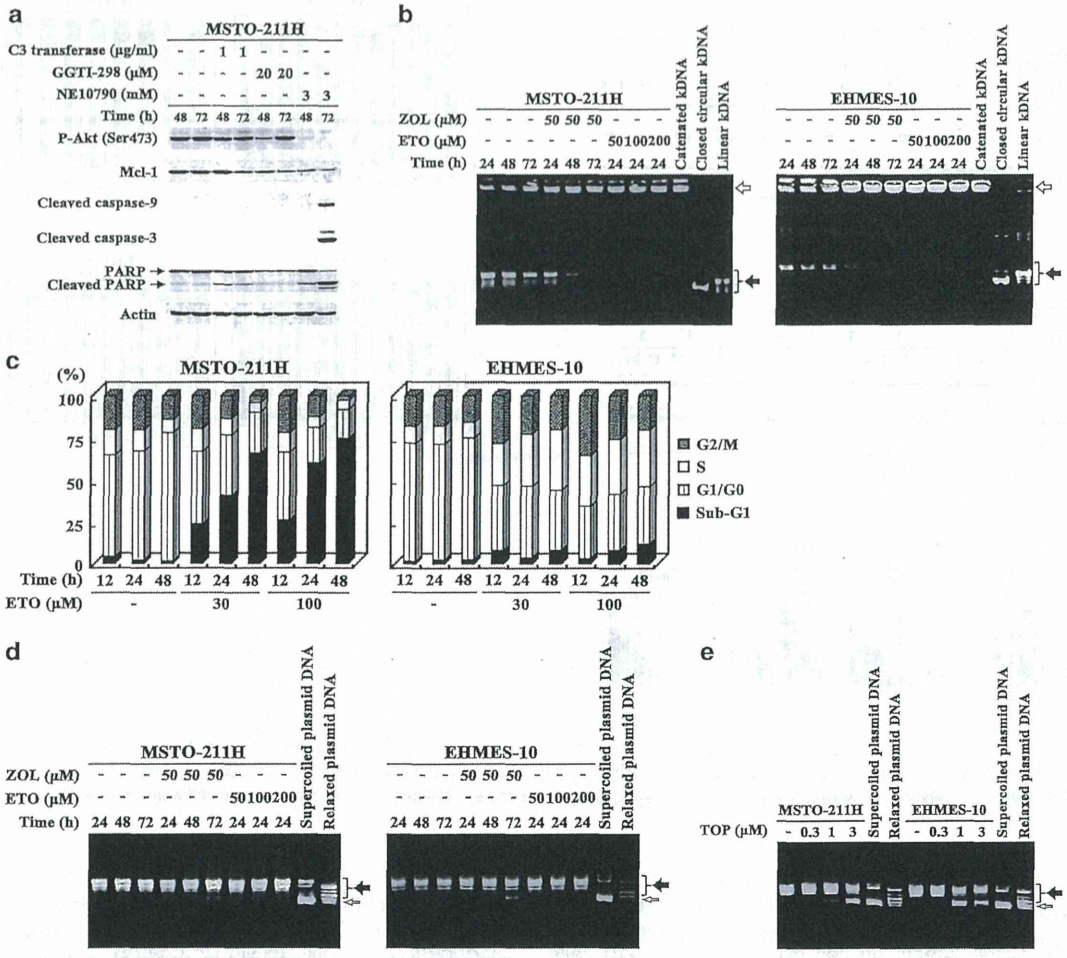

Figure 4 Involvement of geranylgeranylated small G proteins and topoisomerases in apoptosis and S-phase arrest. (**a**) Cells treated with agents as indicated were subjected to western blot analyses. (**b**) Cells treated with agents as indicated were assayed for the Topo II activity with catenated kinetoplast DNA with agarose gel electrophoresis. Open and closed arrows indicate catenated and decatenated kinetoplast DNA, respectively. ETO was used as the control. (**c**) ETO-treated cells were examined for cell cycle with flow cytometry. (**d** and **e**) Cells treated with agents as indicated were assayed for the Topo I activity with supercoiled plasmid DNA. Cells were treated with topotecan (TOP) for 24 h. Open and closed arrows indicate supercoiled and relaxed plasmid DNA, respectively

configurations and being less adhesive to a culture plate (Figure 5a). ZOL treatments caused the changes in time- and dose-dependent manners and the alterations were inhibited with GGOH but not FOH supplement (Supplementary Figure S3). We then examined which small G proteins were responsible for ZOL-mediated changes using the inhibitors. We focused on the round-shaped configuration in EHMES-10 as an indicator of ZOL-induced morphological changes because MSTO-211H cells treated with ZOL became easily detached from a culture plate and thereby were difficult to judge the change. GGTI-298-treated EHMES-10 cells showed almost the same alterations as shown in ZOL-treated cells, whereas NE10790-treated cells did not exhibit the shape changes (Supplementary Figure S4). These data indicated that ungeranylgeranylated Rab family proteins were irrelevant to the ZOL-mediated morphological changes. EHMES-10 cells treated with C3 transferase or Cdc42 siRNA but not with NSC23766 showed the round-shaped morphology although degree of the spheroid shape was lesser than that of GGTI-298-treated cells (Supplementary Figure S5). We also examined actin stress fiber structures as an indicator of the ZOL-induced cytoskeletal deformation (Figure 5b). Phalloidin-stained cells showed that ZOL treatments suppressed the actin stress fiber formation, and that C3 transferase-treated and GGTI-298-treated cells exhibited similar fiber-disrupted patterns. In contrast, NE10790 treatments did not influence the actin stress fiber conformations. These data suggested that morphological changes induced by ZOL treatments were due to inhibition of RhoA and Cdc42.

Discussion

In the present study, we investigated possible molecules responsible for ZOL-induced apoptosis, S-phase arrest and morphological changes in mesothelioma. We examined the

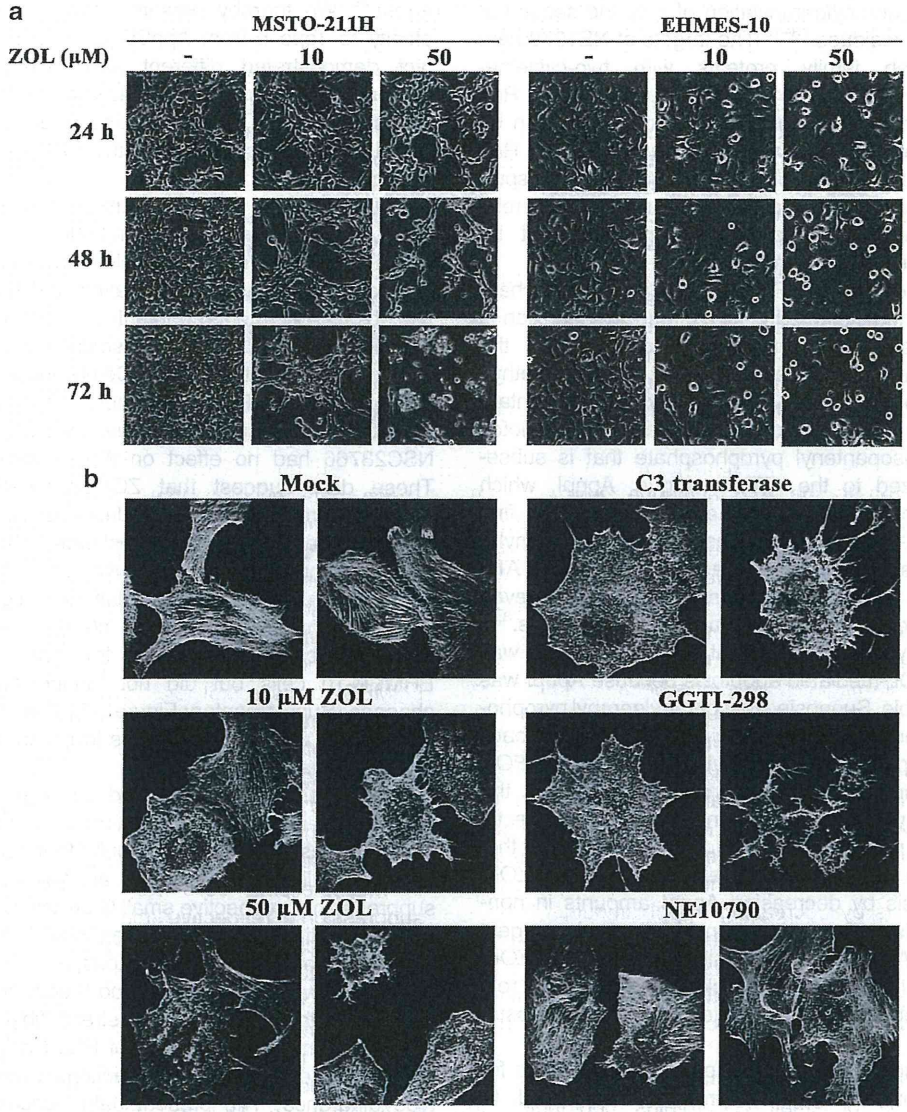

Figure 5 Morphological changes caused by ZOL and small G proteins inhibitors. (**a**) Microphotographs of ZOL-treated cells as indicated (magnification, x 200). (**b**) Structure of actin fibers in EHMES-10 cells which were treated with ZOL, 1 μg/ml C3 transferase, 5 μM GGTI-298 or 1 mM NE10790 for 24 h and were stained with Alexa Fluor 488 phalloidin (magnification, x 630)

target molecules with supplementary isoprenoids, specific inhibitors and siRNA for small G proteins because ZOL-mediated unprenylation of small G proteins resulted in the loss of functions. These experiments collectively indicated that the ZOL-mediated apoptosis and morphological changes were due to inhibition of Rab family and Rho family proteins, respectively. The S-phase arrest observed in ZOL-treated cells was not attributed to unprenylation of small G proteins but to inhibition of Topo II activity.

N-BPs can produce cytotoxic effects, but the precise mechanism remains uncharacterized in particular as for which small G proteins are involved. We examined differential effects of FOH and GGOH and demonstrated that geranylgeranylation was crucial for the cytotoxicity. Treatments with GGTI-298 or NE10790 confirmed that deficient geranylgeranylation induced cell death and we further demonstrated that C3 transferase but not NSC23766 or siRNA for Cdc42 induced cell death. Expression patterns of apoptosis-related molecules indicated that NE10790 but not GGTI-298 or C3 transferase activated the same apoptotic pathways that ZOL did. We thereby concluded that ZOL-induced apoptotic cell death was attributable to the loss of Rab family proteins' functions. A previous study also demonstrated that NE10790 induced apoptosis without cell cycle arrest but did not investigate precise mechanisms as to which apoptosis signals were involved.[12] We did not determine in the present study what kinds of Rab family proteins contributed to ZOL-induced apoptosis, but the experiments with NE10790 narrowed down the targeted Rab family proteins. Rab family proteins possess a one- or two-cysteine-containing motif at the C terminal, and

NE10790 inhibits geranylgeranylation of only the second of the two-cysteines residues.[13–15] The targets of NE10790 are consequently Rab family proteins with two-cysteine-containing motifs such as Rab1, Rab5 and Rab6. Some Rab family proteins are highly expressed in tumors and can be involved in progression and invasion of the tumors.[16,17] Rab family proteins are also involved in intracellular transport among organelles, which is crucial for cell survival. We thereby presume that the Rab functions in tumors cannot be substituted by other small G proteins.

Production of a cytotoxic ATP analogue is another mechanism of ZOL-mediated cytotoxicity.[18] ZOL-induced depletion of isoprenoid can stimulate a feedback mechanism in the mevalonate pathway and enhance the hydroxymethylglutaryl-CoA reductase activity accordingly (Supplementary Figure S1). The upregulated enzyme activity promotes accumulation of isopentenyl pyrophosphate that is subsequently metabolized to the ATP analogue, ApppI, which induces the mitochondria-mediated apoptosis.[18,19] The first generation of non-N-BPs, which does not influence prenylation processes of small G proteins, was converted into an ATP analogue similar to ApppI in the structure and achieved apoptosis by reducing mitochondria membrane potentials.[3,20] The present study, however, did not show that ApppI was responsible for ZOL-mediated apoptosis because ApppI was currently unavailable. Supposing that geranylgeranyl pyrophosphate is an end product and stimulates the feedback mechanism, the present results that GGOH but not FOH cancelled ZOL-mediated effects are consistent with the assumption that ApppI played a role in ZOL-mediated effects. In contrast to the present study, a recent study showed that FOH as well as GGOH supplements suppressed ZOL-mediated apoptosis by decreasing ApppI amounts in non-mesothelioma cells.[21] These data hence collectively suggest that production of ApppI can be a possible mechanism of ZOL-mediated effects although the feedback mechanism and a role of ApppI in the apoptosis are subjected to cell and/or tissue type difference.

The present study indicated that none of the inhibitors for geranylgeranylation of small G proteins contributed to S-phase arrest and showed that the majority of geranylgeranylated small G proteins were irrelevant to increase in S-phase populations. We then examined the possibility that an ATP analogue was responsible for S-phase arrest by inhibiting Topo II activity in mesothelioma. We demonstrated that ZOL specifically suppressed Topo II actions, which is probably mediated by the ATP analogue because Topo II but not Topo I requires ATP for the catalytic activity.[22–24] ETO-treated MSTO-211H and EHMES-10 cells showed apoptosis and S-phase arrest, respectively, as found in ZOL-treated cells. We further investigated whether clodronate, which belongs to the first generation of BPs and produces an ATP analogue, $AppCCl_2p$, similar to ApppI in the structure, induced S-phase arrest in EHMES-10 cells (Supplementary Figure S6). Clodronate treatments reduced cell viability (Supplementary Figure S6a) and augmented sub-G1 populations without S-phase arrest at high concentration in MSTO-211H and EHMES-10 cells (Supplementary Figures S6b and c). Previous studies also showed that clodronate-treated non-mesothelioma cells induced apoptosis but not S-phase arrest.[25] We thereby presume that ApppI has a different affinity to Topo II from $AppCCl_2p$, and a previous study in fact demonstrated different susceptibility of osteoclasts to ApppI and $AppCCl_2p$.[18] ZOL treatments stimulate ApppI accumulations but further studies are required to confirm that ApppI suppresses Topo II activity and induces cell cycle changes.

ZOL treatments induced insufficient adhesion to plates in MSTO-211H cells and round-shape configurations in EHMES-10 cells. GGOH supplements reduced these morphological changes, demonstrating that ungeranylgeranylation of small G proteins contributed to the actions. We showed that GGTI-298 and C3 transferase disturbed formation of actin stress fibers and that siRNA-Cdc42 induced round-shaped configurations in EHMES-10 cells. The GGTI-298-induced alterations were similar to those by ZOL but NE10790 or NSC23766 had no effect on the morphological changes. These data suggest that ZOL-produced changes were resulted from ungeranylgeranylation of Rho family proteins excluding Rac1. We further investigated whether the morphological changes were linked with S-phase arrest because alterations in cell shapes can influence cell growth.[26] NCI-H28 cells, a human mesothelioma cell line, treated with ZOL showed increased S-phase fractions as observed in EHMES-10 cells but did not induce any morphological changes (Supplementary Figure S7). These data implied that induction of S-phase arrest was irrelevant to ZOL-produced morphological changes.

In conclusion, we investigated candidate target molecules of ZOL with inhibitors or siRNA for small G proteins and for topoisomerase enzymes, and found that ZOL-induced effects in mesothelioma cells were associated with functional suppression of respective small G proteins and with inhibition of Topo II activities. Apoptosis was linked with inhibition of Rab family functions and Topo II actions, and S-phase arrest was associated with suppressed Topo II activities. Morphological changes with disrupted actin stress fiber structures were caused by inhibited functions of Rho family protein. Nevertheless, these pharmacological actions were influenced by cell type difference. The present data suggest suitable target molecules for cancer therapy in future and also imply a possible combinatory use of different types of anti-cancer agents for mesothelioma treatments.

Materials and Methods

Cells and reagents. Human mesothelioma, MSTO-211H and NCI-H28 cells, were purchased from American Type Culture Collection (Manassas, VA, USA), and EHMES-1, EHMES-10 and JMN-1B cells were provided by Dr Hamada (Ehime University, Ehime, Japan). ZOL were purchased from Novartis (Basel, Switzerland), and FOH, GGOH, GGTI-298, ETO, topotecan and clodronate were from Sigma-Aldrich (St Louis, MO, USA). C3 transferase and NSC23766 were from Cytoskeleton (Denver, CO, USA) and Merck Millipore (Billerica, MA, USA), respectively. NE10790 were provided by Dr Ebetino FH (Warner Chilcott, Dundalk, Ireland). We purchased siRNA duplex targeting Cdc42 and non-specific control siRNA from Invitrogen (Carlsbad, CA, USA). Transfection of cells with the siRNA was conducted with Lipofectamine RNAiMAX (Invitrogen).

Cell cycle analysis. Cells were fixed in 100% ethanol, treated with RNase (50 μg/ml) and stained with propidium iodide (50 μg/ml). The fluorescence intensity was analyzed with FACSCalibur and CellQuest software (BD Biosciences, San Jose, CA, USA).

Cell proliferation activity. Cell growth was examined with a cell-counting WST kit (Dojindo, Kumamoto, Japan) (WST assay). The amount of formazan produced was determined with the absorbance at 450 nm and the relative viability was calculated based on the absorbance without any treatments.

Western blot analysis. Cells lysates were subjected to sodium dodecyl sulfate polyacrylamide gel electrophoresis and the proteins were transferred to a nitrocellulose membrane. The membrane was hybridized with antibodies against pRb, phosphorylated pRb at Ser 795, Akt, phosphorylated Akt at Ser 473, caspase-3, cleaved caspase-3, caspase-9, cleaved caspase-9, PARP (Cell Signaling, Danvers, MA, USA), Mcl-1, unprenylated Rap1A, Rab6 (Santa Cruz Biotech, Santa Cruz, CA, USA), RhoA, Cdc42, Rac1 (Cytoskeleton), Ras (BD Biosciences) or actin (Sigma-Aldrich). The membranes were developed with the ECL system (GE Healthcare, Buckinghamshire, UK). Membrane and cytoplasm fractions were separated with a native membrane extraction kit (Merck Millipore) according to the manufacturer's protocol. Intensity of hybridized bands was determined with the public domain Image J program (available at http://rsbweb.nih.gov/ij). GTP-binding RhoA and Rac1 proteins were isolated with a pull-down assay using a Rho activation assay biochem kit and a Rac1 activation assay biochem kit (Cytoskeleton) according to the manufacturer's protocol.

Caspase activity. Cells were examined for the caspase-3/7, -8 and -9 activities with respective Caspase-Glo kits according to the manufacturer's protocol (Promega, Madison, WI, USA). The relative activity was calculated based on luminescence intensity of cells without any treatment.

Topoisomerase activity. Topo I and Topo II activities were determined with corresponding kits according to the manufacturer's protocol (TopoGEN, Port Orange, FL, USA). Cell extract and substrate DNA, supercoiled DNA for Topo I or catenated kinetoplast DNA for Topo II, were incubated with (for Topo II activity) and without ATP (Topo I). The reaction mixtures were digested with proteinase K and then subjected to agarose gel electrophoresis.

Immunofluorecence analysis. Cells cultured on a Matrigel (BD biosciences)-coated cover glass were fixed with 3.7% formaldehyde and treated with Alexa Fluor 488 phalloidin (Invitrogen) followed by ProLong Gold antifade reagent (Invitrogen). The fluorescence images were taken with a confocal microscope, Leica TCS-SPE (Leica microsystems, Tokyo, Japan).

Conflict of Interest

The authors declare no conflict of interest.

Acknowledgements. This study was supported by Grants-in-Aid for Scientific Research from the Ministry of Education, Culture, Sports, Science and Technology of Japan, the Grant-in-Aid for Research on seeds for Publicly Essential Drugs and Medical Devices from the Ministry of Health, Labor and Welfare of Japan, and a Grant-in-aid from the Nichias Corporation.

1. Yuasa T, Kimura S, Ashihara E, Habuchi T, Maekawa T. Zoledronic acid-a multiplicity of anti-cancer action. *Curr Med Chem* 2007; **14**: 2126–2135.
2. Frith JC, Mönkkönen J, Blackburn GM, Russell RG, Rogers MJ. Clodronate and liposome-encapsulated clodronate are metabolized to a toxic ATP analog, adenosine 5'-(beta, gamma-dichloromethylene) triphosphate, by mammalian cells in vitro. *J Bone Miner Res* 1997; **12**: 1358–1367.
3. Lehenkari PP, Kellinsalmi M, Näpänkangas JP, Ylitalo KV, Mönkkönen J, Rogers MJ *et al.* Further insight into mechanism of action of clodronate: inhibition of mitochondrial ADP/ATP translocase by a nonhydrolyzable, adenine-containing metabolite. *Mol pharmacol* 2002; **61**: 1255–1262.
4. Luckman SP, Hughes DE, Coxon FP, Graham R, Russell G, Rogers MJ. Nitrogen-containing bisphosphonates inhibit the mevalonate pathway and prevent post-translational prenylation of GTP-binding proteins, including Ras. *J Bone Miner Res* 1998; **13**: 581–589.
5. Wennerberg K, Rossman KL, Der CJ. The Ras superfamily at a glance. *J Cell Sci* 2005; **118**: 843–846.
6. Wright LP, Philips MR. Thematic review series: lipid posttranslational modifications. CAAX modification and membrane targeting of Ras. *J Lipid Res* 2006; **47**: 883–891.
7. Lee MV, Fong EM, Singer FR, Guenette RS. Bisphosphonate treatment inhibits the growth of prostate cancer cells. *Cancer Res* 2001; **61**: 2602–2608.
8. Senaratne SG, Pirianov G, Mansi JL, Arnett TR, Colston KW. Bisphosphonates induce apoptosis in human breast cancer cell lines. *Br J Cancer* 2000; **82**: 1459–1468.
9. Green JR. Antitumor effects of bisphosphonates. *Cancer* 2003; **97**: 840–847.
10. Green JR. Bisphosphonates: preclinical review. *Oncologist* 2004; **9**: 3–13.
11. Okamoto S, Kawamura K, Li Q, Yamanaka M, Yang S, Fukamachi T *et al.* Zoledronic acid produces antitumor effects on mesothelioma through apoptosis and S-phase arrest in p53-independent and Ras prenylation-independent manners. *J Thorac Oncol* 2012; **7**: 873–882.
12. Roelofs AJ, Hulley PA, Meijer A, Ebetino FH, Russell RG, Shipman CM. Selective inhibition of Rab prenylation by a phosphonocarboxylate analogue of risedronate induces apoptosis, but not S-phase arrest, in human myeloma cells. *Int J Cancer* 2006; **119**: 1254–1261.
13. Hutagalung AH, Novick PJ. Role of Rab GTPases in membrane traffic and cell physiology. *Physiol Rev* 2011; **91**: 119–149.
14. Stenmark H, Olkkonen VM. The Rab GTPase family. *Genome Biol* 2001; **2**: REVIEWS3007.
15. Baron RA, Tavaré R, Figueiredo AC, Błazewska KM, Kashemirov BA, McKenna CE *et al.* Phosphonocarboxylates inhibit the second geranylgeranyl addition by Rab geranylgeranyl transferase. *J Biol Chem* 2009; **284**: 6861–6868.
16. Recchi C, Seabra MC. Novel functions for Rab GTPases in multiple aspects of tumour progression. *Biochem Soc Trans* 2012; **40**: 1398–1403.
17. Cheng KW, Lahad JP, Gray JW, Mills GB. Emerging role of RAB GTPases in cancer and human disease. *Cancer Res* 2005; **65**: 2516–2519.
18. Mönkkönen H, Auriola S, Lehenkari P, Kellinsalmi M, Hassinen IE, Vepsäläinen J *et al.* A new endogenous ATP analog (Apppl) inhibits the mitochondrial adenine nucleotide translocase (ANT) and is responsible for the apoptosis induced by nitrogen-containing bisphosphonates. *Br J Pharmacol* 2006; **147**: 437–445.
19. Räikkönen J, Crockett JC, Rogers MJ, Mönkkönen H, Auriola S, Mönkkönen J. Zoledronic acid induces formation of a pro-apoptotic ATP analogue and isopentenyl pyrophosphate in osteoclasts in vivo and in MCF-7 cells in vitro. *Br J Pharmacol* 2009; **157**: 427–435.
20. Rogers MJ, Brown RJ, Hodkin V, Blackburn GM, Russell RG, Watts DJ. Bisphosphonates are incorporated into adenine nucleotides by human aminoacyl-tRNA synthetase enzymes. *Biochem Biophys Res Commun* 1996; **224**: 863–869.
21. Räikkönen J, Mönkkönen H, Auriola S, Mönkkönen J. Mevalonate pathway intermediates downregulate zoledronic acid-induced isopentenyl pyrophosphate and ATP analog formation in human breast cancer cells. *Biochem Pharmacol* 2010; **79**: 777–783.
22. Cortés F, Pastor N. Induction of endoreduplication by topoisomerase II catalytic inhibitors. *Mutagenesis* 2003; **18**: 105–112.
23. Nitiss JL. DNA topoisomerase II and its growing repertoire of biological functions. *Nat Rev Cancer* 2009; **9**: 327–337.
24. Chène P, Rudloff J, Schoepfer J, Furet P, Meier P, Qian Z *et al.* Catalytic inhibition of topoisomerase II by a novel rationally designed ATP-competitive purine analogue. *BMC Chem Biol* 2009; **9**: 1.
25. Forsea AM, Müller C, Riebeling C, Orfanos CE, Geilen CC. Nitrogen-containing bisphosphonates inhibit cell cycle progression in human melanoma cells. *Br J Cancer* 2004; **91**: 803–810.
26. Mammoto A, Huang S, Moore K, Oh P, Ingber DE. Role of RhoA, mDia, and ROCK in cell shape-dependent control of the Skp2-p27kip1 pathway and the G1/S transition. *J Biol Chem* 2004; **279**: 26323–26330.

Supplementary Information accompanies this paper on Cell Death and Disease website (http://www.nature.com/cddis)

Hindawi Publishing Corporation
Journal of Immunology Research
Volume 2015, Article ID 743828, 7 pages
http://dx.doi.org/10.1155/2015/743828

Hindawi

Research Article

Fas Ligand DNA Enhances a Vaccination Effect by Coadministered DNA Encoding a Tumor Antigen through Augmenting Production of Antibody against the Tumor Antigen

Boya Zhong,[1,2] Guangyu Ma,[1] Ayako Sato,[2,3] Osamu Shimozato,[2,4] Hongdan Liu,[2] Quanhai Li,[2,3,5,6] Masato Shingyoji,[7] Yuji Tada,[8] Koichiro Tatsumi,[8] Hideaki Shimada,[9] Kenzo Hiroshima,[10] and Masatoshi Tagawa[2,3]

[1] *Department of Hematology, Fourth Hospital of Hebei Medical University, Shijiazhuang 050035, China*
[2] *Division of Pathology and Cell Therapy, Chiba Cancer Center Research Institute, Chiba 260-8717, Japan*
[3] *Department of Molecular Biology and Oncology, Graduate School of Medicine, Chiba University, Chiba 260-8670, Japan*
[4] *Laboratory of DNA Damage Signaling, Chiba Cancer Center Research Institute, Chiba 260-8717, Japan*
[5] *Department of Immunology, Hebei Medical University, Shijiazhuang 050017, China*
[6] *Cell Therapy Center, 1st Hospital of Hebei Medical University, Shijiazhuang 050031, China*
[7] *Department of Thoracic Diseases, Chiba Cancer Center, Chiba 260-8717, Japan*
[8] *Department of Respirology, Graduate School of Medicine, Chiba University, Chiba 260-8670, Japan*
[9] *Department of Surgery, School of Medicine, Toho University, Tokyo 143-8541, Japan*
[10] *Department of Pathology, Tokyo Women's Medical University Yachiyo Medical Center, Yachiyo 276-8524, Japan*

Correspondence should be addressed to Masatoshi Tagawa; mtagawa@chiba-cc.jp

Received 18 September 2014; Accepted 3 February 2015

Academic Editor: Stuart Berzins

Interaction of Fas and Fas ligand (FasL) plays an important role in the regulation of immune responses by inducing apoptosis of activated cells; however, a possible role of FasL in DNA vaccination has not been well understood. We examined whether administration of DNA encoding *FasL* gene enhanced antitumor effects in mice that were vaccinated with DNA expressing a putative tumor antigen gene, *β-galactosidase* (*β-gal*). Growth of β-gal-positive Colon 26 tumors was retarded in the syngeneic mice immunized with β-gal and FasL DNA compared with those vaccinated with β-gal or FasL DNA. We did not detect increased numbers of β-gal-specific $CD8^+$ T cells in lymph node of mice that received combination of β-gal and FasL DNA, but amounts of anti-β-gal antibody increased with the combination but not with β-gal or FasL DNA injection alone. Subtype analysis of anti-β-gal antibody produced by the combination of β-gal and FasL DNA or β-gal DNA injection showed that IgG2a amounts were greater in mice injected with both DNA than those with β-gal DNA alone, but IgG2b amounts were lower in both DNA-injected than β-gal DNA-injected mice. These data suggest that FasL is involved in boosting humoral immunity against a gene product encoded by coinjected DNA and enhances the vaccination effects.

1. Introduction

DNA vaccine holds an advantage over conventional types which use a target protein as an immunogen in the stability and its relatively low systemic toxicity and has been examined for the efficacy in experimental animal models and moreover in clinical settings [1, 2]. Previous studies demonstrated that administration of DNA potentially induced immune responses to an antigen encoded by the DNA and produced protective immunity [3, 4]. Nevertheless, the low transduction efficacy with DNA vaccine administered *in vivo* hampered extensive clinical application. A possible use of

a molecular adjuvant, which can be also administered as DNA, can circumvent the inefficient transduction level [5, 6].

Fas ligand (FasL), type II transmembrane protein, is a member of tumor necrosis factor family with 40 kDa and plays a major role in inducing programmed cell death when it is interacted with Fas [7]. The Fas/FasL interactions induce apoptosis of immune cells including T, B cells and macrophages and the cell death is often associated with activated stages of immune cells. The activation-induced cell death is a mechanism to inhibit excessive immune responses and to terminate ongoing immunity. Naive T cells come to express FasL upon antigen stimulation, and the activated T cells are subjected to apoptosis, which ceases the T cells-mediated responses [8]. Moreover, expression of FasL contributed to enhanced antigen uptake in dendritic cells [9], which indicates that FasL are involved not only in decreasing immunity but in augmenting immune responses. The Fas/FasL interactions thus regulate immune responses in multiple ways.

In the present study, we examined a role of FasL expression as an adjuvant in vaccination effects on tumor growth. We used β-galactosidase (β-gal) that was used as a putative tumor antigen in a murine animal model and tested whether administration of FasL DNA modulated antitumor responses induced by immunization of β-gal-encoding DNA.

2. Materials and Methods

2.1. Cells and Mice. Murine colon carcinoma Colon 26 cells and packaging cells, Ψ2 and PA317, were maintained with RPMI1640 or DMEM medium supplemented with 10% fetal calf serum. BALB/c mice were purchased from CLEA Japan SLC (Tokyo, Japan).

2.2. Transduction of Tumor Cells. The retrovirus vector LXSN (provided by Dr. A.D. Miller, Fred Hutchinson Cancer Research Center, Seattle, WA, USA) was used to harbor β-gal cDNA. The retroviral DNA was transfected into ecotropic Ψ2 cells and the cell-free supernatants were further incubated with amphotropic PA317 cells. The culture supernatants of PA317 cells were used for infecting Colon 26 cells. Transduction of Colon 26 cells with the *β-gal* gene (Colon 26/β-gal) was confirmed with 5-bromo-4-chloro-3-indolyl β-D-galactoside (X-gal) staining.

2.3. DNA Administration and X-Gal Staining. Full-length β-gal, mouse FasL cDNAs were cloned into expression plasmid vectors, pcDNA3 (the transgene is activated by cytomegalovirus promoter) or pCAGGS (CAG promoter), respectively, and plasmid DNA of pcDNA3/β-gal, pCAGGS/FasL was purified with an endotoxin-free DNA extraction kit (Qiagen, Hilden, Germany). Cardiotoxin (Latoxan, Valence, France) was injected into thigh muscle of mice 5 days before DNA administration. For investigation of β-gal expression, DNA (10 μg or 50 μg) was injected in the same area in thigh, and the muscles were fixed with 2% formaldehyde and 0.05% glutaraldehyde and then reacted with X-gal solution [10].

2.4. Antitumor Effects Produced by DNA Injection. BALB/c mice were injected with cardiotoxin (1 μmol) and with pcDNA3/β-gal and/or pCAGGS/FasL DNA (50 μg each) on day 5. They were subcutaneously inoculated with Colon 26/β-gal cells (1×10^6) 21 days after DNA injections, and the tumor volume was calculated according to the formula ($1/2 \times$ length $\times$ width^2). All the animal experiments were approved by the Animal Experiment and Welfare Committee at Chiba Cancer Center Research Institute.

2.5. Detection of Antigen-Specific T Cell Population. A specific epitope peptide sequence TPHPARIGL of β-gal for H-2L^d haplotype was loaded onto the soluble dimeric H-2L^d-linked immunoglobulin (Ig) complex (Dimer X I, BD Bioscience, San Jose, CA, USA) [11]. Inguinal lymph node cells were reacted with fluorescence isothiocyanate- (FITC-) conjugated anti-mouse CD8 antibody (Ab) (BD Bioscience) and with the dimeric H-2L^d-linked Ig complexes loaded with the peptide, followed by phycoerythrin-conjugated anti-mouse IgG_1 (BD Bioscience). The dimeric complex-positive or -negative and CD8$^+$ T cells were examined with FACSCalibur (BD Bioscience) and CellQuest software (BD Bioscience).

2.6. Detection of Anti-β-Gal Antibody. Amounts of anti-β-gal Ab were estimated with enzyme-linked immunosorbent assay (ELISA) using purified β-gal protein (Invitrogen, Carlsbad, CA, USA) as a standard and horseradish peroxidase- (HRP-) conjugated anti-mouse IgG Ab (GE Healthcare, Buckinghamshire, UK) as previously described [12]. An isotype of anti-β-gal Ab in mice sera was detected with HRP-conjugated anti-mouse IgG_1 (SouthernBiotech, Birmingham, AL, USA), IgG_{2a}, IgG_{2b}, or IgM (Invitrogen) Ab. The values of respective isotypes were calculated based on optical density at 450 nm since isotype-specific standard anti-β-gal Ab is currently unavailable.

2.7. Statistical Analysis. We conducted statistical analyses with the one-way analysis of variance (ANOVA) and P values less than 0.05 were judged as significant.

3. Results

3.1. Immunization with DNA Encoding β-Gal Gene. We examined expression of the *β-gal* gene in muscles of mice that were injected with pcDNA3/β-gal plasmid DNA and investigated a possible enhancement of the gene expression with a cardiotoxin treatment (Figure 1). Cardiotoxin destroys muscle tissues and the regeneration process facilitates uptake of DNA [13, 14]. Expression levels of β-gal detected with the X-gal staining method depended on amounts of pcDNA3/β-gal DNA used, and the cardiotoxin treatment prior to DNA administration augmented the β-gal expression. We thereby treated mice with cardiotoxin and 5 days later immunized the mice with 50 μg DNA in the following experiments.

3.2. Enhanced Antitumor Effects by FasL DNA Immunization. We investigated whether immunization with DNA encoding

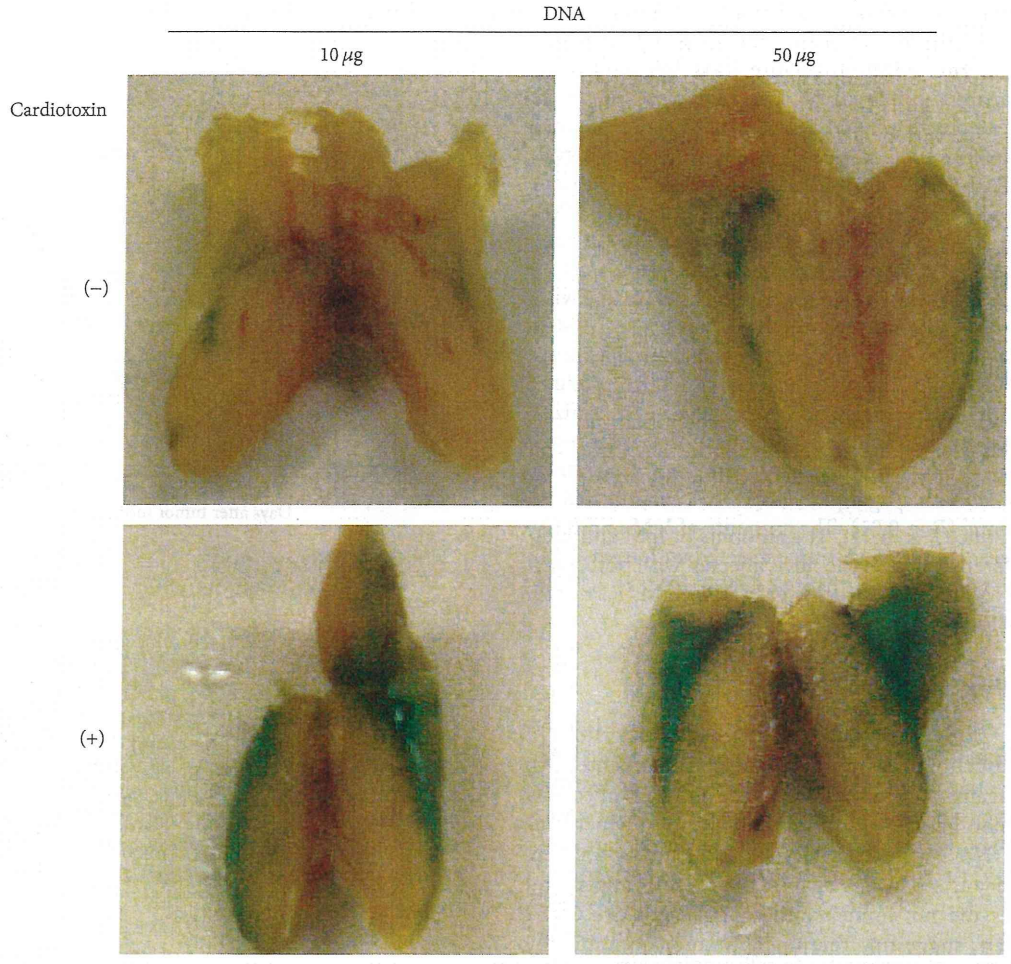

FIGURE 1: Expression of β-gal protein in mice that received DNA immunization. BALB/c mice were injected with or without cardiotoxin at thigh muscles and then with pcDNA3/β-gal (10 or 50 μg) at the same muscles 5 days later. The thigh muscles were stained with the X-gal staining 5 days after DNA immunization.

a putative tumor antigen achieved antitumor effects. We firstly transduced murine Colon 26 cells with the *β-gal* gene and confirmed that the growth of Colon 26/β-gal cells *in vitro* and *in vivo* was not different from parental Colon 26 cells. Syngeneic BALB/c mice were injected with cardiotoxin and then with DNA expressing the *β-gal* and/or *FasL* gene or vector DNA as a control. The mice were then inoculated with Colon 26/β-gal cells and the tumor volumes were monitored. Growth of Colon 26/β-gal cells was not statistically different among mice that were inoculated with vector DNA, pcDNA3/β-gal, or pCAGGS/FasL DNA (Figure 2), and the tumor growth in these mice was not different from that in naive mice (data not shown). In contrast, the tumor growth in mice that received both pcDNA3/β-gal and pCAGGS/FasL DNA was retarded compared with that in mice immunized with vector DNA, pcDNA3/β-gal, or pCAGGS/FasL DNA ($P < 0.05$). These data indicated that immunization of DNA encoding the *β-gal* or the *FasL* gene alone did not produce antitumor effects but a combinatory use of both DNA achieved vaccination effects.

3.3. Constant Frequency of Antigen-Specific T Cells. We investigated a possible mechanism underlying the antitumor effects produced by the combinatory immunization. We firstly examined induction of antigen-specific $CD8^+$ T cells that mediated cytotoxic activities. Cells from inguinal lymph nodes that were obtained on days 7, 14, and 21 after DNA immunization were stained with antibody against CD8 Ab and peptide-loaded class I antigens (Figures 3(a) and 3(b)). Immunization of both *β-gal* and FasL DNA did not increase the antigen-positive $CD8^+$ T cells compared with other DNA immunizations or naive cases irrespective of days examined. We also calculated total $CD8^+$ cell numbers in lymph nodes and found that the numbers in mice which received both *β-gal* and FasL DNA did not increase compared with those in other experimental groups (Figure 3(c)). These data suggest that cytotoxic T cells were not responsible for the antitumor effects by immunization of β-gal and FasL DNA.

3.4. Increased Ab against β-Gal. We examined a possible involvement of humoral immunity in the antitumor effects

by the immunization of β-gal and FasL DNA. We firstly measured serum concentrations of anti-β-gal IgG Ab produced by DNA immunization (Figure 4(a)). Injection of β-gal DNA increased anti-β-gal Ab as demonstrated between the group injected with pcDNA3/β-gal + pCAGGS DNA and that with pcDNA3 + pCAGGS DNA ($P < 0.05$), whereas injection of FasL DNA did not (pcDNA3 + pCAGGS/FasL versus pcDNA3 + pCAGGS, $P = 0.48$). Coinjected FasL DNA together with β-gal DNA however augmented the Ab production since the group injected with pcDNA3/β-gal + pCAGGS/FasL DNA showed greater responses than that with pcDNA3 + pCAGGS/FasL or pcDNA3/β-gal + pCAGGS DNA ($P < 0.01$). We then further examined a possible influence of FasL DNA injection on differential Ig isotype production (Figure 4(b)). IgG_{2a} amounts were greater in immunization with both β-gal and FasL DNA than in that with β-gal DNA alone ($P < 0.01$), whereas IgG_{2b} amounts were rather less in the injection of β-gal plus FasL DNA than in that of β-gal DNA alone ($P < 0.01$). The amounts of IgM and IgG_1 were not different between the mice injected with both β-gal and FasL DNA and those with β-gal DNA (IgM; $P = 0.29$, IgG_1; $P = 0.85$).

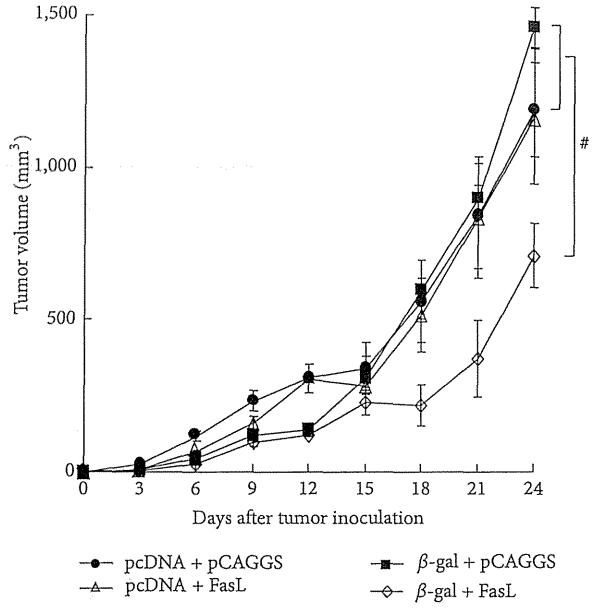

FIGURE 2: Antitumor effects produced by DNA immunization. BALB/c mice ($n = 6$ or 7) were treated with cardiotoxin and 5 days later with DNA (50 μg for each), pcDNA3 + pCAGGS, pcDNA3 + pCAGGS/FasL (FasL), pcDNA3/β-gal (β-gal) + pCAGGS, or pcDNA3/β-gal + pCAGGS/FasL (β-gal + FasL). The mice were then inoculated with Colon 26/β-gal cells (1×10^6) 21 days after DNA injections. The tumor growth of mice injected with cDNA3/β-gal + pCAGGS/FasL was significantly retarded 21 days after the tumor inoculation compared with that of mice inoculated with pcDNA3 + pCAGGS, pcDNA3 + pCAGGS/FasL, or pcDNA3/β-gal + pCAGGS. $^{\#}P < 0.05$.

4. Discussion

The present study demonstrated that administration of FasL DNA functioned as an adjuvant and augmented Ab production against a tumor antigen. The adjuvant effects by FasL expression generated antitumor immunity which was primed by DNA vaccination targeting the tumor antigen. A combinatory use of DNA against the tumor antigen and FasL however did not influence the antigen-positive $CD8^+$ T cell numbers, suggesting that the antitumor immunity by DNA vaccine was not attributable to cell-mediated immunity. In contrast, previous studies showed that vaccination of a tumor antigen with plasmid DNA achieved antitumor effects through antigen-positive cytotoxic T cells [15]. Moreover, the Fas/FasL interactions have negative effects on efficacy of DNA vaccine not only by inducing apoptosis of cytotoxic T cells [16] but also by promoting clearance of injected plasmid DNA [17]. Nevertheless, Dharmapuri et al. demonstrated that downregulation of Fas with siRNA did not influence the antitumor responses produced by DNA encoding a tumor antigen although siRNA for Bakl or caspase-8, both of which were involved in apoptotic processes, enhanced the responses in the same experimental settings [18]. A possible role of FasL and Fas in the context of DNA vaccine *in vivo* is thus subjected to multiple factors such as immunological microenvironments where tumors develop.

The present study did not examine a role of $CD4^+$ T cells but the population can be involved in DNA vaccine-mediated antitumor responses in which $CD8^+$ populations did not play a central role [19]. We however demonstrated that the FasL DNA administration augmented production of anti-β-gal IgG Ab and IgG_{2a} Ab specific for a tumor antigen. Enhanced anti-β-gal Ab production suggested involvement of Ab-dependent cellular cytotoxicity that involved Ab binding to Fc receptors and/or complement-dependent cellular cytotoxicity that activated complement cascades. The previous study by Dharmapuri et al. also indicated that antitumor responses augmented by coinjected siRNA for Bakl or caspase-8 were attributable to class switch from IgG_1 to IgG_{2a} [18]. In fact, IgG_{2a} bound to Fc receptors better than other isotypes in a murine system [20]. In addition, comparison among immunoglobulin subtypes which, respectively, have a similar affinity to same antigen showed that IgG_{2a} activated complement greater than IgG_{2b} [21]. Nimal et al. showed increased T helper type 2 rather than T helper type 1 cell responses in vaccination with *FasL* gene-fused DNA and demonstrated that IgG_{2a} production was greater than IgG_1 without generating T cell responses [22]. The data were concordant with the current study although their vaccination targets viral infections. The present data together with the previous studies collectively imply that expressed FasL at local DNA injection sites facilitated not only Ab production but also class switching, which resulted in augmentation of Ab-mediated cytotoxic reactions. Nevertheless, a precise mechanism of how the FasL molecules enhanced the humoral immunity is currently unknown. Cardiotoxin at the injection sites may also contribute to the humoral immunity since the treatment induces inflammatory reactions with local cytokine productions [14]. Proinflammatory cytokines such